TECHNICAL ARTICLE

Structural and optical properties of $Ba_3(Nb_{6-x}Ta_x)Si_4O_{26}$ ($x = 0.6$, 1.8, 3.0, 4.2, 5.4)

W. Wong-Ng ⓘ,[1] G. Y. Liu ⓘ,[2,a)] W. F. Liu,[3] Y. Q. Yang,[1,4] S. Y. Wang,[5] Y. C. Lan,[6] D. A. Windover,[1] and J. A. Kaduk ⓘ[7,8]

[1]*Materials Measurement Science Division, National Institute of Standards and Technology, Gaithersburg, MD 20899, USA*
[2]*State Key Laboratory of Geological Processes and Mineral Resources, and Institute of Earth Sciences, China University of Geosciences, Beijing 100083, China*
[3]*Tianjin Key Laboratory of Low Dimensional Materials Physics and Preparing Technology, School of Science, Tianjin University, Tianjin 300072, China*
[4]*Material School of Science and Engineering, JiangXi University of Science and Technology, GanZhou 341000, China*
[5]*College of Physics and Material Science, Tianjin Normal University, Tianjin 300074, China*
[6]*Department of Physics and Engineering Physics, Morgan State University, Baltimore, MD 21251, USA*
[7]*Department of Chemistry, Illinois Institute of Technology, Chicago, IL 60616, USA*
[8]*Department of Physics, North Central College, Naperville, IL 60540, USA*

Structure and optical properties have been successfully determined for a series of niobium- and tantalum-containing layered alkaline-earth silicate compounds, $Ba_3(Nb_{6-x}Ta_x)Si_4O_{26}$ ($x = 0.6$, 1.8, 3.0, 4.2, 5.4). The structure of this solid solution was found to be hexagonal P-$62m$ (No. 189), with $Z = 1$. With x increases from 0.6 to 5.4, the lattice parameter a increases from 8.98804(8) to 9.00565 (9) Å and c decreases from 7.83721(10) to 7.75212(12) Å. As a result, the volume decreases from 548.304(11) to 544.479(14) Å^3. The $(Nb/Ta)O_6$ distorted octahedra form continuous chains along the c-axis. These $(Nb/Ta)O_6$ chains are in turn linked with the Si_2O_7 groups to form distorted pentagonal channels in which Ba ions were found. These Ba^{2+} ions have full occupancy and a 13-fold coordination environment with neighboring oxygen sites. Another salient feature of the structure is the linear Si–O–Si chains. When x in $Ba_3(Nb_{6-x}Ta_x)Si_4O_{26}$ increases, the bond valence sum (BVS) values of the Ba sites increase slightly (2.09–2.20), indicating the size of the cage becoming progressively smaller (over-bonding). While SiO cages are also slightly smaller than ideal (BVS range from 4.16 to 4.19), the $(Nb/Ta)O_6$ octahedral cages are slightly larger than ideal (BVS range from 4.87 to 4.90), giving rise to an under-bonding situation. The bandgaps of the solid solution members were measured between 3.39 and 3.59 eV, and the $x = 3.0$ member was modeled by density functional theory techniques to be 3.07 eV. The bandgaps of these materials indicate that they are potential candidates for ultraviolet photocatalyst. © 2019 International Centre for Diffraction Data. [doi:10.1017/S0885715619000745]

Key words: $Ba_3(Nb_{6-x}Ta_x)Si_4O_{26}$ ($x = 0.6$, 1.8, 3.0, 4.2, 5.4), X-ray powder reference diffraction patterns, photocatalysts

I. INTRODUCTION

In recent years, there has been much renewed interest in silicate materials for photocatalyst applications. Silicate ceramics are versatile materials which have a variety of industrial applications. Besides electrical engineering/electronics, automotive engineering, hot air technology, and telecommunication applications, they can also be used for lighting and optical technology (Paranthaman et al., 2015) and are potential photocatalytic materials. Neatu *et al.* (2014) have used three different cobalt-containing silicates with different structures to evaluate their photocatalytic activities under different conditions, either for the overall water splitting under UV irradiation in the absence of sacrificial electron donor or for hydrogen generation under simulated sunlight illumination

in the presence of methanol. Based on the report that $Ag_6Si_2O_7$ was found to be a silicate photocatalyst for the visible region (Lou et al., 2014), we have recently studied the Ba $(Zn,Co)SiO_4$ series (Anike *et al.*, 2019) and found that all solid solution members except for $BaCoSiO_4$ all have a bandgap of >3.0 eV, rendering them to be potentially suitable in the UV light region.

The demands for optics and optoelectronics for fiber and waveguide materials with nonlinear optical properties have promoted much research interest for glass-ceramic oxide materials that are capable of producing optical second-harmonic generation. For example, the structural dependence of the luminescence of niobite silicate compound, $K_2(NbO)_2Si_4O_{12}$, has been studied by Blasse (1980) and Blasse *et al.* (1989, 1991, 1992) and by Crosnier *et al.* (1992). Especially interesting has been silicates with efficient luminescence where niobite groups with one short Nb–O distance occur. The importance of this short Nb–O distance and

---
a)Author to whom correspondence should be addressed. Electronic mail: guangyaoliu@hotmail.com

its importance for the luminescence has been explained by the molecular orbital (MO) calculations by Hazenkamp and Blasse (1993) and Hazenkamp et al. (1993). The compound $K_3(NbO_2)_3Si_2O_7$, which is built with covalent networks of SiO_4 tetrahedra and MO_6 octahedra, has been studied extensively by Choisnet et al. (1976) and Launay et al. (1974). Shannon and Katz (1970) and Choisnet et al. (1976) further investigated the structure of $A_3(NbO_2)_6Si_4O_{14}$ and $A_3(TaO_2)_6Si_4O_{14}$ ($A = Ba$, Sr) for the nonlinear optical, fast alkali-ion mobility, ion-exchange, and potential photocatalysis applications.

The main goal of this study is to determine the detailed structures of the silicate solid solution of $Ba_3((Nb,Ta)O_2)_6Si_4O_{14}$ to provide an accurate basis for bandgap computation. The second goal is to measure and validate with calculations their bandgaps in order to determine whether the materials have the potential applications in the visible light range or ultra-violet light range. Furthermore, since X-ray diffraction (XRD) is a nondestructive technique for phase identification (McMurdie et al., 1986), X-ray diffraction reference patterns are critical for phase characterization; therefore, another goal of this investigation is to determine the experimental patterns for $Ba_3(Nb_{6-x}Ta_x)Si_4O_{26}$ ($x = 0.6$, 1.8, 3.0, 4.2, 5.4) and to make them widely available through submission to the Powder Diffraction File (PDF) (2019).

II. EXPERIMENTAL

A. Sample preparation

The white powders were prepared from stoichiometric amounts of $BaCO_3$, Nb_2O_5, Ta_2O_5, and SiO_2 using solid-state high-temperature techniques. The starting samples were mixed, pelletized, and heat treated in the air at 800 °C for 10 h and subsequently annealed at 1100 °C for 12 h, 1200 °C for 36 h with intermediate grindings, and 1300 °C for another 15 h with intermediate grindings. During each heat treatment in air, the samples were furnace cooled. The heat treatment process was repeated until no further changes were detected in the powder X-ray diffraction patterns.

B. Estimation of composition using X-ray fluorescence

The estimation of composition for samples of $Ba_3(Nb_{6-x}Ta_x)Si_4O_{26}$ ($x = 0.6$, 1.8, 3.0, 4.2, 5.4) were performed on a Bruker M4 Tornado micro X-ray fluorescence instrument. A Rh X-ray source, set to 50 kV and 300 µA, with a 20 µm mono-capillary were used for excitation (S.N. 2001495). A Bruker XFlash 450 µm thick, Silicon Drift Detector (S.N. 11881_0239) was used for data collection for the scans. Each spectrum used a minimum peak sum of over 40,000 X-ray counts per analyzed element, reducing counting statistics as a source of uncertainty below all other contributions. Analysis were performed using Bruker Quantify version 1.3.1.3327 with standard Spectrum Elements method and calibrated for our instrument (S.N. 6099). For each sample, 18 independent, 60 second live time measurements were performed, and the variance of the composition derived from these measurements were used for error analysis.

C. X-ray Rietveld refinements and powder reference patterns

The pressed wafers of $Ba_3(Nb_{6-x}Ta_x)Si_4O_{26}$ ($x = 0.6$, 1.8, 3.0, 4.2, 5.4) were mounted in modeling clay, or (where the wafers were not available) as acetone slurries on zero-background cells. The X-ray powder patterns were measured (5–130° 2θ, 0.020 214 4° steps, 1 s step^{-1}, Cu$K\alpha$ radiation at 300 K) on a Bruker D2 Phaser diffractometer equipped with a LynxEye detector. (The purpose of identifying the equipment and computer software in this article is to specify the experimental procedure. Such an identification does not imply recommendation or endorsement by the National Institute of Standards and Technology.)

The Rietveld refinement technique (Rietveld, 1969) with the software suite GSAS (Larson and von Dreele, 2004) was used to determine the structure of the $Ba_3(Nb_{6-x}Ta_x)Si_4O_{26}$ ($x = 0.6$, 1.8, 3.0, 4.2, 5.4) series. The structure of $Ba_3Ta_6Si_4O_{26}$ (PDF 04-011-0699) was used as the starting model for the refinements. Reference patterns were obtained with a Rietveld pattern decomposition technique. Using this technique, the reported peak intensities were derived from the extracted integrated intensities and positions calculated from the lattice parameters. The pseudo-Voight function (profile function #4) was used for the refinement of both series of compounds (Thompson et al., 1987; Finger et al., 1994); Stephens, 1999). When peaks are not resolved at the resolution function, the intensities are summed, and an intensity-weighted d-spacing is reported. In summary, these patterns represent ideal specimen patterns.

D. Bond valence sum calculations

The bond valence sum values, BVS, for Ba, Ta, Nb, and Si sites were calculated using the Brown–Altermatt empirical expression (Brown and Altermatt, 1985; Brese and O'Keeffe, 1991). The BVS of an atom i is defined as the sum of the bond valences v_{ij} of all the bonds from atoms i to atoms j. The most commonly adopted empirical expression for the bond valence v_{ij} as a function of the interatomic distance d_{ij} is $v_{ij} = \exp[(R_0 - d_{ij})/B]$. The parameter, B, is commonly taken to be a "universal" constant equal to 0.37 Å. The values for the reference distance R_0 for Ba–O, Nb–O, Ta–O, and Si–O are 2.29, 1.911, 1.92, and 1.624, respectively (Brown and Altermatt, 1985; Brese and O'Keeffe, 1991). In the sites, where there are more than two different types of atoms, the BVS value is the weighted sum of the fraction of occupancy.

E. Bandgap measurements and calculations

The optical properties of the $Ba_3(Nb_{6-x}Ta_x)Si_4O_{26}$ ($x = 0.6$, 1.8, 3.0, 4.2, 5.4) compounds were investigated by measuring the UV–visible absorption spectra by using a Shimadzu UV-3600 UV-VIS-NIR spectrophotometer.

Bandgap calculations were conducted using the density functional theory (DFT) approach. We use the linearized augmented plane wave (LAPW) method for the computation of the electronic structure. The calculations were performed using the Elk package (2019). The generalized gradient approximation (GGA) was used for the correlation and exchange potentials (Perdew et al., 1996). The atomic sphere radii that we used were 2.5 a.u. for Ba, 1.91 a.u. for Nb and Ta, and 1.39 and 1.62 a.u. for Si and O, respectively (Blaha et al., 1990). The RK_{max} parameter was set to be 5.5. Self-interaction corrections for d electrons are introduced by an on-site Coulomb and exchange interactions, namely the Hubbard and exchange parameter U and J, with $U = 0.187$,
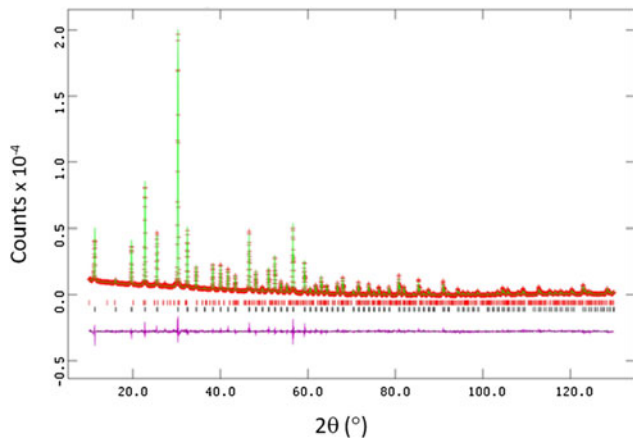
Figure 1. Observed (crosses), calculated (solid line), and difference XRD patterns (bottom) for $Ba_3(Ta_3Nb_3)Si_4O_{26}$ by a Rietveld analysis technique. The difference pattern is plotted at the same scale as the other calculated peak positions. The small peak in the 2θ around the 28° region is the K_β peak of the 110 reflection. Its presence does not interfere with the refinement.

$J = 0.039$ Ry for Nb, $U = 0.173$ and $J = 0.036$ Ry for Ta, according to the report by Solovyev *et al.* (1994). The energy convergence criteria are 10^{-5} Ry, and the charge convergence criteria are 10^{-3}.

III. RESULTS AND DISCUSSION

During the atomic Nb/Ta concentration ratio calculations for $Ba_3(Nb_{6-x}Ta_x)Si_4O_{26}$ ($x = 0.6, 1.8\ 3.0, 4.2, 5.4$) using the X-ray fluorescence technique, the Ba concentration was assumed to be 3. Our results confirm the ratio of the concentration of Nb/Ta to be in reasonable agreement with the intended compositions within 1.5 σ (standard deviations),

TABLE I. Rietveld refinement residuals for $Ba_3(Nb_{6-x}Ta_x)Si_4O_{26}$ [P-$62m$ (No. 189), $Z = 1$].

Composition	R_{wp}	R_p	χ^2
$Ba_3(Nb_{5.4}Ta_{0.6})Si_4O_{26}$	0.0758	0.0568	1.78
$Ba_3(Nb_{4.2}Ta_{1.8})Si_4O_{26}$	0.0704	0.0549	1.60
$Ba_3(Nb_3Ta_3)Si_4O_{26}$	0.0579	0.0423	1.86
$Ba_3(Nb_{1.8}Ta_{4.2})Si_4O_{26}$	0.0558	0.0426	1.56
$Ba_3(Nb_{0.6}Ta_{5.4})\ Si_4O_{26}$	0.0533	0.0376	1.46

TABLE II. Cell parameters for $Ba_3(Nb_{6-x}Ta_x)Si_4O_{26}$ ($x = 0.6$–5.4), space group P-$62m$ (No. 189), $Z = 1$., and D_{cal} represents calculated density

Chemical formula	a (Å)	c (Å)	V (Å)	D_{cal} (g cm^{-3})
$Ba_3(Nb_{5.4}Ta_{0.6})$ Si_4O_{26}	8.988 04(8)	7.837 21(10)	548.304(11)	4.70
$Ba_3(Nb_{4.2}Ta_{1.8})$ Si_4O_{26}	8.993 33(8)	7.814 76(12)	547.377(12)	5.02
$Ba_3(Nb_3Ta_3)$ Si_4O_{26}	8.998 61(10)	7.7902(2)	546.295(11)	5.36
$Ba_3(Nb_{1.8}Ta_{4.2})$ Si_4O_{26}	9.001 89(9)	7.767 37(13)	545.095(13)	5.69
$Ba_3(Nb_{0.6}Ta_{5.4})$ Si_4O_{26}	9.0056 5(9)	7.752 12(12)	544.479(14)	6.02

D_{cal} represents calculated density.

TABLE III. Bond distances and BVS values for $Ba_3(Nb_3Ta_3)Si_4O_{26}$, P-$62m$ (No. 189), $Z = 1$.

Atom	Atom	Bond distances (Å)	BVS values
(1) $Ba_3(Nb_{5.4}Ta_{0.6})Si_4O_{26}$			
Ba_1	O7	2.816(8) × 2	2.090
	O8	2.857(5) × 4	
	O8	3.071(6) × 4	
	O9	3.455(12)	
	O9	3.113(2) × 2	
Nb_2/Ta_3	O6	1.939(2)	4.868
	O7	1.972(2) × 2	
	O8	2.020(3) × 2	
	O9	2.021(2)	
Si_4	O5	1.604(3)	4.180
	O8	1.609(2) × 3	
(2) $Ba_3(Nb_{4.2}Ta_{1.8})Si_4O_{26}$			
Ba_1	O7	2.826(7) × 2	2.105
	O8	2.836(5) × 4	
	O8	3.089(6) × 4	
	O9	3.453(10)	
	O9	3.114(2) × 2	
Nb_2/Ta_3	O6	1.930(2)	4.886
	O7	1.980(2) × 2	
	O8	2.020(3) × 2	
	O9	2.017(2)	
Si_4	O5	1.600(3)	4.166
	O8	1.612(2) × 3	
(3) $Ba_3(Nb_3Ta_3)Si_4O_{26}$			
Ba_1	O7	2.831(9) × 2	2.115
	O8	2.839(6) × 4	
	O8	3.068(7) × 4	
	O9	3.481(13)	
	O9	3.113(2) × 2	
Nb_2/Ta_3	O6	1.924(3)	4.894
	O7	1.986(2) × 2	
	O8	2.021(3) × 2	
	O9	2.017(3)	
Si_4	O5	1.602(3)	4.160
	O8	1.612(2) × 3	
(4) $Ba_3(Nb_{1.8}Ta_{4.2})Si_4O_{26}$			
Ba_1	O7	2.812(8) × 2	2.155
	O8	2.826(5) × 4	
	O8	3.081(7) × 4	
	O9	3.482(11)	
	O9	3.113(2) × 2	
Nb_2/Ta_3	O6	1.922(2)	4.903
	O7	1.993(2) × 2	
	O8	2.023(2) × 2	
	O9	2.008(2)	
Si_4	O5	1.601(3)	
	O8	1.609(2) × 3	4.188
(5) $Ba_3(Nb_{0.6}Ta_{5.4})\ Si_4O_{26}$			
Ba_1	O7	2.812(8) × 2	2.200
	O8	2.828(5) × 4	
	O8	3.043(7) × 4	
	O9	3.512(11)	
	O9	3.110(2) × 2	
Nb_2/Ta_3	O6	1.938(2)	4.888
	O7	1.994(2) × 2	
	O8	2.028(2) × 2	
	O9	1.995(2)	
Si_4	O5	1.609(3)	4.157
	O8	1.610(2) × 3	

The ideal BVS values are 2.0 (Ba site), 5.0 (mixed Nb/Ta site), and 4.0 (Si site), respectively. The values for the reference distance R_0 for Ba–O, Nb–O, Ta–O, and Si–O are 2.29, 1.911, 1.92, and 1.624, respectively (Brown and Altermatt, 1985; Brese and O'Keeffe, 1991).

namely, 6.57(0.72)/0.533(0.058) for $Ba_3(Nb_{5.4}Ta_{0.6})Si_4O_{26}$, 6.08(1.72)/1.91(0.54) for $Ba_3(Nb_{4.2}Ta_{1.8})Si_4O_{26}$, 3.34(0.46)/3.03(0.41) for $Ba_3(Nb_3Ta_3)Si_4O_{26}$, 1.96(0.2)/4.24(0.44) for $Ba_3(Nb_{1.8}Ta_{4.2})Si_4O_{26}$, and 0.65(0.84)/5.37(0.69) for $Ba_3(Nb_{0.6}Ta_{5.4})Si_4O_{26}$. The numbers inside the brackets represent 1 σ.

A. Structure of $Ba_3(Nb_{6-x}Ta_x)Si_4O_{26}$

Figure 1 gives the plots of Rietveld refinements for $Ba_3(Nb_3Ta_3)Si_4O_{26}$, as an example, where observed (crosses), calculated (solid line), and difference XRD patterns (bottom) are shown. The tick marks indicate the calculated peak positions, and the difference pattern is plotted on the same scale as other patterns. The refinement results are shown in Table I. A small amount of impurity phases has been found with a few of the phases. For example, 2.6% of $Ba_{1.31}O_{15.63}Ta_{5.63}$ was found to coexist with $Ba_3(Nb_{1.8}Ta_{4.2})Si_4O_{26}$. The atomic coordinates and displacement parameters of $Ba_3(Nb_{6-x}Ta_x)Si_4O_{26}$ ($x = 0.6, 1.8, 3.0, 4.2, 5.4$) are given in Supplementary Table SI. Tables II and III summarize the lattice parameters, bond distances, and BVS values. Selected bond angles concerning the $(Nb/Ta)O_6$ octahedra and the SiO_4 tetrahedra are given in Supplementary Table SII.

The materials crystallize in the space group of $P\text{-}62m$ (No. 189), $Z = 1$. Lattice parameters and calculated density D_x are reported in Table II. It is seen that as the Ta content increases from $x = 0.6$–5.4, the lattice parameter a increases from $a = 8.988\,04(8)$ to $9.005\,65(9)$ Å, while c decreases from $7.837\,21(10)$ to $7.752\,12(12)$ Å, giving rise to a slight decrease in the cell volume from 548.304(11) to 544.479(14) Å^3. As expected, the D_x values increase from 4.70 to 6.02 g cm^{-3} as the size of ionic radius, $r(R^{3+})$ (Shannon, 1976) decreases. Compositional dependence of the unit cell volume, V, for $Ba_3(Nb_{6-x}Ta_x)Si_4O_{26}$ is given in Figure 2, and a monotonic decrease of V is observed.

The structure of $Ba_3(Nb_{6-x}Ta_x)Si_4O_{26}$ viewed along the c-axis and a-axis is shown in Figures 3 and 4. The atomic labeling schemes are shown in Supplementary Figures S1 and S2. The structure consists of corner-shared distorted SiO_4 tetrahedra and $(Nb/Ta)O_6$ octahedra. In Figure 4, it is seen that the rings of three cornered-linked $(Nb,Ta)O_6$ octahedra are linked to form continuous chains, and these chains, in turn, are held together by Si_2O_7 groups (or two corner-shared

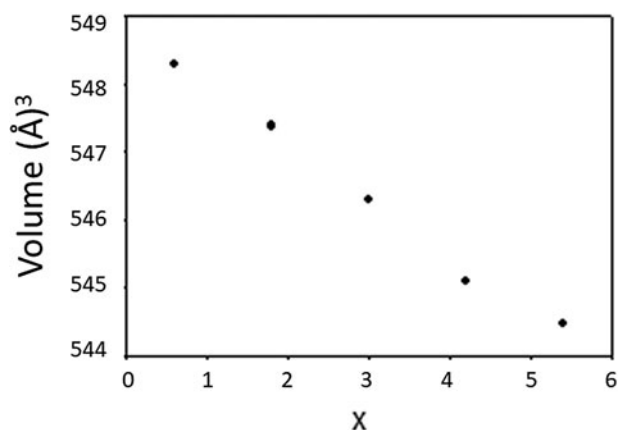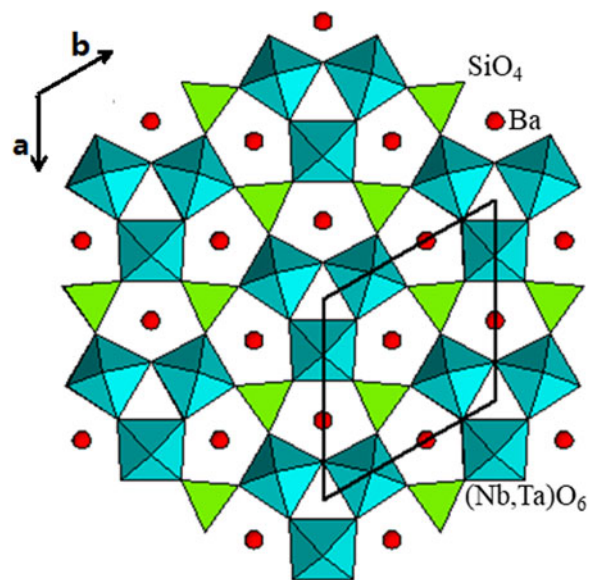Figure 3. [001] Projection of the crystal structure of $Ba_3(Nb_{6-x}Ta_x)Si_4O_{26}$ showing the Ba-filled distorted fivefold coordination channels.

SiO_4 tetrahedral units). The Si and Nb/Ta sites all have distorted environments (Table III). The Si–O distances exhibit a narrow spread from 1.600(3) to 1.612(2) Å. In the distorted $(Nb/Ta)O_6$ octahedral environment, one of the Nb–O distances is particularly short (1.922(2)–1.939(2) Å) as compared with the rest (1.972(2)–2.028(2) Å). This observation agrees with that reported in $K_2(NbO)_2Si_4O_{12}$ (Blasse et al., 1992) as one of the prerequisites to be an efficient luminescence material.

The coordination number (C.N.) for all Ba sites is 13 for the five $Ba_3(Nb_{6-x}Ta_x)Si_4O_{26}$ compounds, and the environment of each Ba site is a distorted pentagonal prism. In Figure 3, Ba atoms are situated inside a distorted pentagonal channel. Among the 13 Ba–O distances, 10 of them range from 2.812(8) to 3.089(6) Å, while the other three are longer, ranging from 3.110(2) to 3.512(11) Å.

Another structure feature of the $Ba_3(Nb_{6-x}Ta_x)Si_4O_{26}$ series is the linearity of the Si–O–Si groups. Apparently, there have been disputes in literature about the reality of this angle. For example, Liebau considered the reported linearity

Figure 2. Compositional dependence of the unit cell volume, V, for $Ba_3(Nb_{6-x}Ta_x)Si_4O_{26}$. A monotonic decrease of V is observed.
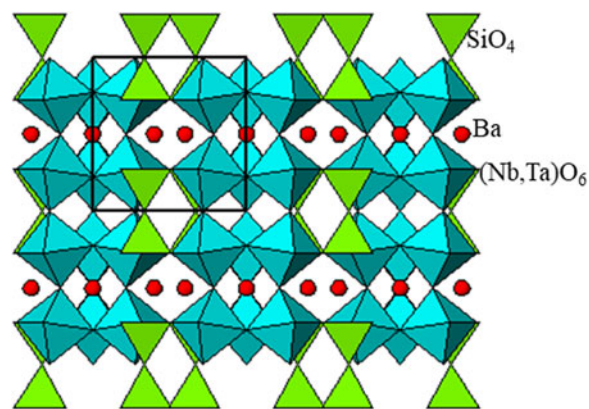

Figure 4. [100] Projection of the crystal structure of $Ba_3(Nb_{6-x}Ta_x)Si_4O_{26}$ derived from the X-ray powder data, showing cornered-shared $(Ta,Nb)O_6$ octahedra and SiO_4 tetrahedra.

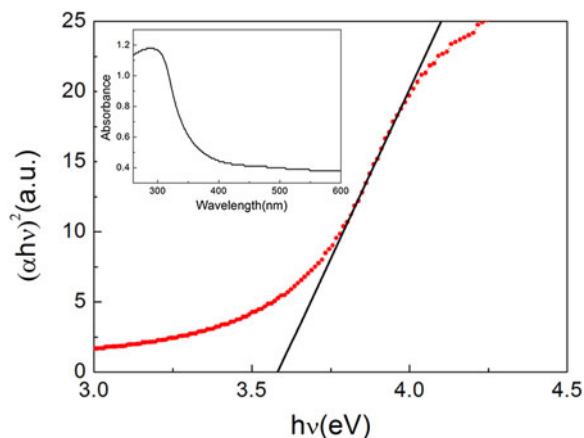Figure 5. UV–visible absorption spectra of the as-synthesized $Ba_3(Nb_3Ta_3)Si_4O_{26}$, and Tauc plot for calculating bandgaps E_g by extrapolation of the linear portion of the plots of $(\alpha h\nu)^2$ vs. $h\nu$. Insert is the corresponding absorbance curve.

Figure 6. Structural model used for the DFT calculations for the sample $Ba_3(Nb_3Ta_3)Si_4O_{26}$.

was due to a wrong symmetry assignment. A number of other authors also reported the observed linear Si–O–Si groups (Zoltai and Buerger, 1959; Cruickshank, 1961; Cruickshank *et al.*, 1962; Launay *et al.*, 1974). In our compounds, the Si–O5–Si angles are all 180° (Supplementary Table SII). Apparently, the Si–O–Si angles are very flexible in silicate-type of compounds. The Si–O–Si bond angles in low-pressure crystalline structures vary from 134° to 150°, with some extremes near 160°. In α-quartz and α-cristobalite, the Si–O–Si bond angles are around 144°, with average Si–O bond lengths of 1.61 Å (Yuan and Cormack, 2003).

The BVS values of the Ba site were found to increase when the x value increases (Table III). For example, when $x = 0.6$, 1.8, 3.0, 4.2, 5.4, the BVS values increase from 2.090, 2.105, 2.115, 2.155 to 2.200. All these values are somewhat greater than the ideal value of 2.0, indicating over-bonding situation, or the cage size is too small. The BVS values for the Si sites are all similar and are all slightly greater than the ideal value of 4.0 (ranging from 4.16 to 4.19), indicating over-bonding situation. For the Nb/Ta sites, all BVS values are slightly less than 5.0, suggesting under-bonding (cage too large).
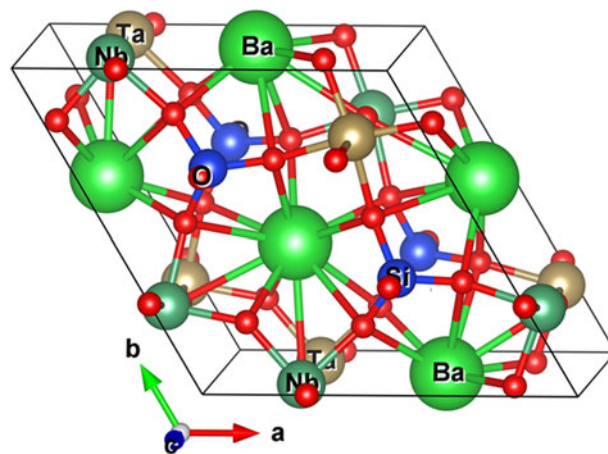
B. Optical properties of $Ba_3(Nb_{6-x}Ta_x)Si_4O_{26}$

Figure 5 and Supplementary Figures S3–S6 provide the UV–visible absorption spectra of the five $Ba_3(Nb_{6-x}Ta_x)Si_4O_{26}$ ($x = 0.6$, 1.8, 3.0, 4.2, 5.4) compounds. There is a strong absorption peak around 300 nm for all these samples. The optical bandgaps E_g corresponding to the energy separation can be estimated via the direct allowed inter-band transition (Qasrawi, 2005) between the maxima of the valence band and the minima of conduction band using the Tauc's law (Tauc *et al.*, 1966):

$$\alpha h\nu = A(h\nu - E_g)^n$$

where A is a constant that depends on the transition probability, $h\nu$ is the energy of incident photons, and n is an index that characterizes the optical absorption process. The values of $n = 2$, 1/2, 3, and 3/2 correspond to allowed indirect, allowed direct, forbidden indirect, and forbidden direct bandgap, respectively. The value of $n = ½$ was employed in our work to calculate the bandgaps.

The bandgaps E_g of $Ba_3(Nb_{6-x}Ta_x)Si_4O_{26}$ ($x = 0.6$, 1.8, 3.0, 4.2, 5.4) were obtained by extrapolating the linear portion of the plot to $(\alpha h\nu)^2 = 0$. An example of $x = 3.0$ is shown in
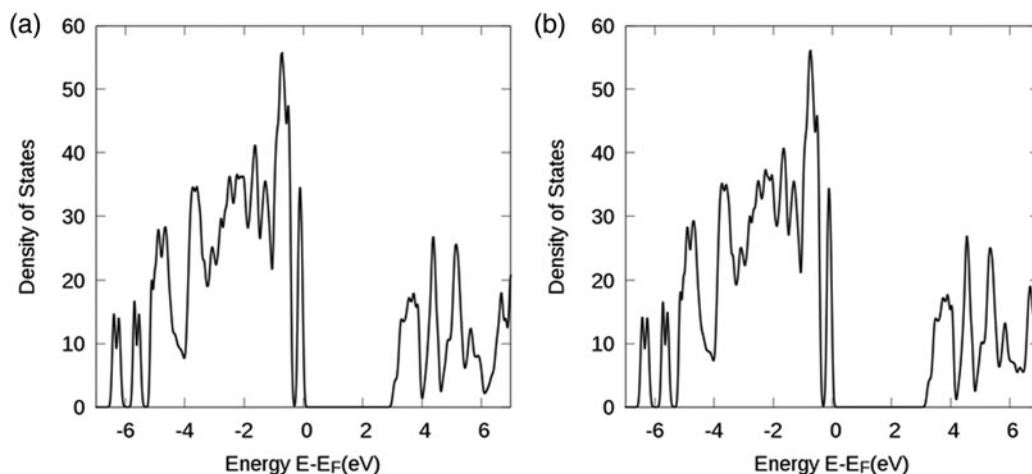

Figure 7. Density of states vs. $E - E_F$ plot for $Ba_3(Nb_3Ta_3)Si_4O_{26}$: (a) With GGA and (b) with GGA + U approaches. E_F stands for the Fermi energy level.

TABLE IV. X-ray reference powder diffraction pattern of $Ba_3(Nb_3Ta_3)Si_4O_{26}$ [P-$62m$ (No. 189), $a = 8.998\ 61(10)$ Å, $c = 7.7902(2)$ Å, $V = 546.295(11)$ Å^3, and $D_x = 5.36$ g cm^{-3}].

d_{cal}	I_{obs}	h	k	l		d_{cal}	I_{obs}	h	k	l	
7.7914	211	1	0	0	M	7.7914	211	0	0	1	M
5.5095	15	1	0	1		4.4993	151	1	1	0	
3.8959	398	1	1	1	+	3.4845	216	2	0	1	M
3.4844	216	1	0	2	M	2.9452	999	2	1	0	M
2.9452	999	1	1	2	M	2.7548	237	2	1	1	M
2.7548	237	2	0	2	M	2.5974	88	3	0	0	M
2.5974	88	0	0	3	M	2.4643	5	3	0	1	
2.3494	103	2	1	2		2.2494	107	2	2	0	M
2.2494	107	1	1	3	M	2.1613	88	3	1	0	+
2.0827	62	3	1	1		1.9479	285	0	0	4	+
1.8899	91	3	1	2	M	1.8899	91	1	0	4	M
1.8365	24	3	0	3		1.7876	118	3	2	0	M
1.7876	118	1	1	4	M	1.7425	168	4	0	2	+
1.7006	50	4	1	0	M	1.7006	50	2	2	3	M
1.6613	39	4	1	1	M	1.6613	39	3	1	3	M
1.6247	322	3	2	2	M	1.6247	322	2	1	4	M
1.5585	150	4	1	2	+	1.5283	20	5	0	1	.
1.4998	44	3	3	0	.	1.4725	85	2	2	4	+
1.4469	43	3	1	4	+	1.3996	57	5	1	0	M
1.3996	57	3	3	2	M	1.3774	93	4	0	4	+
1.3364	21	5	0	3		1.3171	71	5	1	2	M
1.3171	71	3	2	4	M	1.2987	6	3	3	3	
1.2809	67	4	1	4	+	1.2640	24	4	3	1	M
1.2640	24	3	1	5	M	1.2476	55	5	2	0	M
1.2476	55	1	1	6	M	1.2318	14	2	0	6	
1.2169	54	4	3	2	M	1.2169	54	5	0	4	M
1.1883	126	3	3	4	+	1.1746	55	4	2	4	+
1.1614	4	3	0	6		1.1489	13	4	3	3	M
1.1489	13	4	1	5	M	1.1367	97	6	1	2	M
1.1367	97	5	1	4	M	1.1247	21	4	4	0	+
1.1131	36	3	1	6	+	1.1020	9	5	3	1	M
1.1020	9	5	0	5	M	1.0806	82	4	4	2	+
1.0704	13	4	2	5	+	1.0506	35	5	2	4	M
1.0506	35	3	2	6	M	1.0412	15	6	2	2	M
1.0412	15	2	1	7	M	1.0321	14	4	1	6	+
1.0231	5	7	1	1	+	1.0145	19	6	1	4	
0.9978	4	5	4	0	+	0.9895	5	4	3	5	M
0.9895	5	3	1	7	M	0.9818	22	6	3	0	M
0.9818	22	3	3	6	M	0.9740	54	4	2	6	+
0.9666	37	5	4	2	M	0.9666	37	5	3	4	M
0.9592	3	7	1	3	.	0.9519	27	5	1	6	+
0.9450	56	6	2	4	+	0.9247	85	7	2	2	M
0.9247	85	2	1	8	M	0.9184	12	6	3	3	.
0.9120	44	4	4	5	+	0.9058	31	5	0	7	+
0.8997	42	5	5	0	M	0.8997	42	5	2	6	M
0.8938	24	2	2	8	+	0.8880	56	8	1	2	+
0.8767	99	6	1	6	+	0.8711	33	8	0	4	M
0.8711	33	4	0	8	M	0.8605	15	8	1	3	M
0.8605	15	7	1	5	M	0.8553	69	7	3	2	+

The symbols "M" and "+" refer to peaks containing contributions from two and more than two reflections, respectively. The particular peak that has the strongest intensity in the entire pattern is assigned an intensity of 999, and other lines are scaled relative to this value. The d-spacing values are the calculated values from refined lattice parameters, and "I" represents integrated intensity values.

Figure 5. The plots for samples with $x = 0.6, 1.8, 4.2, 5.4$ are shown in Supplementary Figures S1–S4. The bandgap values, E_g, are between 3.39 and 3.59 eV, and they increase slightly with x. The Nb/Ta ratio appears to affect the bandgap value insignificantly. From these values, it is clear that the $Ba_3(Nb_{6-x}Ta_x)Si_4O_{26}$ phases ($x = 0.6, 1.8, 3.0, 4.2, 5.4$) have wide bandgaps over 3.0 eV and will only absorb near-ultraviolet portion (300–400 nm or 3.10–4.13 eV) of the solar radiation. Therefore, the $Ba_3(Nb_{6-x}Ta_x)Si_4O_{26}$ materials are potential candidates for UV photocatalysts. Substitution of Nb by Ta does not have a significant effect on the E_g values.

Figure 6 gives the structural model for the DFT calculation for $Ba_3(Nb_3Ta_3)\ Si_4O_{26}$. The density of states vs. $E-E_F$ plots for $Ba_3(Nb_3Ta_3)Si_4O_{26}$ using GGA and GGA + U approaches are shown in Figures 7(a) and 7(b). After including the Coulomb and exchange interactions, the bandgaps have slightly increased from an E_g value of 2.85 eV to a value of 3.07 eV. This value, while lower than the experimental value of about 3.58 eV, could be considered as acceptable. According to Perdew (1986), using the DFT approach, the bandgap values of transition metal and rare-earth containing compounds were often calculated to be lower than the

experimental values (Perdew, 1986). With an orbital-dependent on-site Coulomb interaction (U) and exchange interaction (J), one can somewhat improve the results. However, it is still notable that for compounds with partially-occupied d- or f-orbitals, the calculated bandgaps are still underestimated using local density approximation or GGA techniques.

C. Reference X-ray diffraction pattern

1989 gives the reference pattern for $Ba_3(Ta_3Nb_3)Si_4O_{26}$. In this pattern, the symbols "M" and "+" refer to peaks containing contributions from two and more than two reflections, respectively. The particular peak that has the strongest intensity in the entire pattern is assigned an intensity of 999, and other lines are scaled relative to this value. In general, the d-spacing values are calculated values from refined lattice parameters. The intensity values reported are integrated intensities (rather than peak heights) based on the corresponding profile parameters as reported in Table IV. For resolved, overlapped peaks, intensity-weighted calculated d-spacing, along with the observed integrated intensity and the hkl indices of both peaks (for "M"), or the hkl indices of the strongest peak (for "+") are used. For peaks that are not resolved at the instrumental resolution, the intensity-weighted average d-spacing and the summed integrated intensity value are used. In the case of a cluster, unconstrained profile fits often reveal the presence of multiple peaks, even when they are closer than the instrumental resolution. In this situation, both d-spacing and intensity values are reported independently. All patterns have been submitted for inclusion in the PDF.

D. Summary

A solid solution of the series $Ba_3(Nb_{6-x}Ta_x)Si_4O_{26}$ ($x = 0.6, 1.8, 3.0, 4.2, 5.4$) has been prepared successfully, and their crystal structures have been determined. $Ba_3(Nb_{6-x}Ta_x)Si_4O_{26}$ crystallizes in the hexagonal symmetry with the space group of P-$62m$ (No. 189), with $Z = 1$. The structure consists of rings of three cornered-linked $(Nb,Ta)O_6$ octahedra linked to form continuous chains along the c-axis, the chains, in turn, are held together by Si_2O_7 groups. Another structure feature is the linear Si–O–Si chains found among the Si_2O_7 groups. The bandgap values (allowed direct electronic transitions) were between 3.39 and 3.59 eV. The Nb/Ta ratio affect the bandgap value only slightly. These $Ba_3(Nb_{6-x}Ta_x)Si_4O_{26}$ materials are potential candidates for UV photocatalysts. The X-ray powder diffraction patterns of the $Ba_3(Nb_{6-x}Ta_x)Si_4O_{26}$ ($x = 0.6, 1.8, 3.0, 4.2, 5.4$) series have been submitted to be included in the PDF.

SUPPLEMENTARY MATERIAL

The supplementary material for this article can be found at https://doi.org/10.1017/S0885715619000745

Anike, J., Derbushi, R., Wong-Ng, W., Liu, W., King, N., Wang, S., Kaduk, J. A., and Lan, Y. (2019). "Crystallographic and band gap measurements of Ba(Co$_{1-x}$Zn$_x$)SiO$_4$ (x = 0.2, 0.4, 0.6, 0.8)," Powder Diffr. **34**, 242–250.

Blaha, P., Schwarz, K., Sorantin, P., and Trickey, S. B. (1990). "Full-potential, linearized augmented plane-wave programs for crystalline systems," Comput. Phys. Commun. **59**, 399–415.

Blasse, G. (1980). "The luminescence of closed-shell transition-metal complexes: new development," Struct. Bond. **42**, 1–41.

Blasse, G., Dirksen, G. J., Hazenkamp, M. F., Verbaere, A., and Oyetloa, S. (1989). "A luminescent and a non-luminescent modification of cesium phosphatoniobate," Eur. J. Solid State Inorg. Chem. **26**, 497–503.

Blasse, G., Dirksen, G. J., Crosnier, M. P., and Pitfard, Y. (1991). "Luminescence of siliconiobates," Eur. J. Solid State Inorg. Chem. **28**, 425–429.

Blasse, G., Dirksen, G. J., Crosnier, M. P., and Pitfard, Y. (1992). "The luminescence of K$_2$(NbO)$_2$Si$_4$O$_{12}$," J. Alloy. Compd. **189**, 259–261.

Brese, N. E. and O'Keeffe, M. (1991). "Bond-valence parameters for solids," Acta Crystallogr. B. **47**, 192–197.

Brown, I. D. and Altermatt, D. (1985). "Bond-valence parameters obtained from a systematic analysis of the inorganic crystal-structure database," Acta Crystallogr. B. **41**, 244–247.

Choisnet, J., Nguyen, N., Groult, D., and Raveau, B. (1976). "De nouveaux oxydes a reseau forme d'octaedres NbO$_6$ (TaO$_6$) et de groupes Si$_2$O$_7$: les phases A$_3$Ta$_6$Si$_4$O$_{26}$ (A = Ba, Sr) et K$_6$M$_6$Si$_4$O$_{26}$ (M = Nb, Ta)," Mat. Res. Bull. **11**, 887–894.

Crosnier, M. P., Guyomard, D., Verbaere, A., Pitffard, Y., and Tournoux, M. (1992). "The potassium niobyl cyclotetrasilicate K$_2$(NbO)$_2$Si$_4$O$_{12}$," J. Solid State Chem. **98**, 128–132.

Cruickshank, D. W. J. (1961). "The role of 3d-orbitals in π-bonds between (a) silicon, phosphorous, sulphur or chlorine and (b) oxygen or nitrogen," J. Chem. Soc., 5486–5504.

Cruickshank, D. W. J., Lynton, H., and Barclay, G. A. (1962). "A reinvestigation of the crystal structure of thortveitite Sc$_2$Si$_2$O$_7$," Acta Cryst. **15**, 491–498.

Elk (2019). Elk is an all-electron full-potential linearised augmented-plane wave (LAPW) code with many advanced features. Written originally at Karl-Franzens-Universität Graz as a milestone of the EXCITING EU Research and Training Network. The code is freely available under the GNU General Public License (vs. 5.2.14; June 21, 2019).

Finger, L. W., Cox, D. E., and Jephcoat, A. P. (1994). "A Correction for powder diffraction peak asymmetry due to axial divergence," J. Appl. Cryst. **27**, 892–900.

Hazenkamp, M. F. and Blasse, G. (1993). "Can luminescence spectroscopy contribute to the elucidation of surface species," Res. Chem. Intermediat. **19**, 343–354.

Hazenkamp, M. F., van Duijneveldt, F. B., and Blasse, G. (1993). "Theoretical-study on the intensities of charge-transfer type transitions in VO$_{4(3-)}$ and VOF$_3$," Chem. Phys. **169**, 55–63.

International Centre for Diffraction Data (2019). PDF-4+2019 (Database), edited by Dr. Soorya Kabekkodu, International Centre for Diffraction Data, Newtown Square, PA, USA.

Larson, A. C. and von Dreele, R. B. (2004). "General Structure Analysis System (GSAS)," Los Alamos National Laboratory Report LAUR 86-748, Los Alamos, USA.

Launay, S., Mahé, P., and Quarton, M. (1974). "Synthesis and crystal data for K$_3$Nb$_3$O$_6$Si$_2$O$_7$," Powder Diffr. **9**(2), 96–97.

Lou, Z., Huang, B., Wang, Z., Ma, X., Zhang, R., Zhang, X., Qin, X., Dai, Y., and Whangbo, M.-H. (2014). "Ag$_6$Si$_2$O$_7$: a silicate photocatalyst for the visible region," Chem. Mater. **26**, 3873–3875.

McMurdie, H. F., Morris, M. C., Evans, E. H., Paretzkin, B., Wong-Ng, W., Ettlinger, L., and Hubbard, C. R. (1986). "JCPDS—International centre for diffraction data task group on cell parameter refinement," Powder Diffr. **1**(2), 66–76.

Neatu, S., Puche, M., Fornes, V., and Garcia, H. (2014). "Cobalt-containing layered or zeolitic silicates as photocatalysts for hydrogen generation," Chem. Commun. **50**, 14643–14646.

Paranthaman, M. P., Wong-Ng, W., and Bhattacharya, R. N. (2015). *Springer Series in Materials Science 218, Semiconductor Materials for Solar Photovoltaic Cells* (Springer, New York).

Perdew, J. P. (1986). "Density functional theory and the band gap problem," Int. J. Quantum Chem. Quantum Chem. Symp. **19**, 497–523.

Perdew, J., Burke, K., and Ernzerhof, M. (1996). "Generalized gradient approximation made simple," Phys. Rev. Lett. **77**, 3865–3868.

Qasrawi, A. F. (**2005**). "Refractive index, band gap and oscillator parameters of amorphous GaSe thin films," Cryst. Res. Technol. **40**(6), 610–614.

Rietveld, H. M. (**1969**). "A profile refinement method for nuclear and magnetic structures," J. Appl. Cryst. **2**, 65–71.

Shannon, R. D. (**1976**). "Revised effective ionic radii and systematic studies of interatomic distances in halides and chalcogenides," Acta Crystallogr. A. **32**, 751–767.

Shannon, J. and Katz, L. (**1970**). "The structure of barium silicon niobium oxide, $Ba_3Si_4Nb_6O_{26}$: a compound with linear silicon–oxygen–silicon groups," Acta Cryst. B. **26**, 105–109.

Solovyev, I. V., Dederichs, P. H., and Anisimov, V. I. (**1994**). "Corrected atomic limit in the local-density approximation and the electronic-structure of d-impurities in Rb," Phys. Rev. B. **50**, 16861–16871.

Stephens, P. W. (**1999**). "Phenomenological model of anisotropic peak broadening in powder diffraction," J. Appl. Cryst. **32**, 281–289.

Tauc, J., Grigorovici, R., and Vancu, A. (**1966**). "Optical properties and electronic structure of amorphous germanium," Phys. Status Solidi B. **15**, 627–637.

Thompson, P., Cox, D. E., and Hastings, J. B. (**1987**). "Rietveld refinement of Debye–Scherrer synchrotron X-ray data from Al_2O_3," J. Appl. Cryst. **20**, 79–83.

Yuan, X. and Cormack, A. N. (**2003**). "Si–O–Si bond angle and torsion angle distribution in vitreous silica and sodium silicate glasses," J. Non-Crystalline Solids. **319**(1–2), 31–43.

Zoltai, T. and Buerger, M. J. (**1959**). "The crystal structure of coesite, the dense, high-pressure form of silica," Z. Kristallogr. **111**, 129–141.